Journal of Alloys and Compounds, 182 (1992) 115–130
JALCOM 136

The mediated electrochemical dissolution of plutonium oxide: kinetics and mechanism*

Yury Zundelevich
Chemistry and Materials Science, L-367, Lawrence Livermore National Laboratory, Livermore, CA 94550 (USA)

(Received August 21, 1991; in final form October 1, 1991)

Abstract

The design and optimization of large-scale systems for electrochemical dissolution of PuO_2 in the presence of Ag^{2+} ions acting as mediators require a knowledge of true dissolution kinetics, usually obscured by limiting capacities of the electrolytic cells. Analysis conducted in this study identified the PuO_2 surface reaction with silver(II) as the rate-controlling step and led to a mathematical model of the process based on first-order heterogeneous kinetics. By applying the model for simulation of a large-scale PuO_2 dissolution experiment reported by Bourges *et al.*, a first-order rate constant $k = 0.0004$ cm min^{-1} for electrochemical dissolution of PuO_2 at 25 °C has been determined. The model was then used to demonstrate the strong effects of the PuO_2 size distribution, the silver(I) concentration, the anodic current and some other operational parameters on the dissolution time and the current efficiency. The results of this investigation provide a means for rational design and operation of plutonium-processing systems and stress the importance of operation at the limiting current.

1. Introduction

The dissolution of PuO_2 in aqueous solutions of HNO_3 by means of Ag^{2+} ions electrochemically generated at the anode of the electrolytic cell is becoming a method of choice in the plutonium-processing industry, replacing a much slower process involving a mixture of nitric and hydrofluoric acids. The speed of the new process is such that, virtually all observed trends reported so far [1–4] – linearity in time, apparent independence of solids' surface area and proportionality (up to a limit) to the anodic current – point to Ag^{2+} generation as the only rate-limiting step of the entire process.

If the high rate of dissolution itself is taken for granted, as the above references seem to imply, then the dissolution step ought to be looked upon merely as a sink for Ag^{2+} ions, whatever its true kinetics may be. However, the same data [1–4] which support the notion of an extremely high dissolution rate contain evidence that this rate is in fact far from infinite. Even for the highly reactive submicron PuO_2 particles used in these experiments, the

*Paper presented at 15th Actinide Separations Conference, Charleston, SC, June 17–21, 1991.

quasi-linear plots of dissolution *vs.* time exhibit pronounced curvature toward the end of the run, demonstrating that, despite the increased silver(II) concentration at that stage, the reduction in the solid surface area does eventually slow the dissolution rate. This clearly would not be observed if the dissolution process were instantaneous.

Fine submicron powders usually present handling problems and, if feasible, are turned into coarser materials with sizes ranging from a few microns to tens of microns. For these less reactive materials there is even less reason for taking for granted their high electrochemical dissolution rate. Their optimum processing (minimum dissolution time at maximum current efficiency) may involve, for example, consideration of a feedback between the rate of generation and the rate of consumption of Ag^{2+} ions and would not be possible without prior knowledge of the dissolution kinetics. Finally, neither modeling nor process optimization, involving mixed materials, in which PuO_2 needs to be leached from inert matrices, can be accomplished meaningfully without understanding first the mechanism of electrochemical dissolution of pure PuO_2.

These are but a few examples demonstrating the need for understanding the mechanism(s) of electrochemical dissolution of plutonium oxide as well as the oxides of some other actinides. Following the usual practice, our description of the dissolution process — be it the reaction or diffusion kinetics, taking place at the surface or away from it — will be regarded as adequate, once a given combination of steps leads to the results consistent with available data. In particular, the dissolution rates obtained on a basis of any of the above assumptions will be checked against the data. Unavoidably, some important but unnecessary modeling details will be ignored in the process.

2. Mechanism of electrochemical dissolution of plutonium oxide

The electrochemical dissolution of PuO_2 resulting in the formation of solvable plutonyl(VI) ion PuO_2^{2+} proceeds through electron transfer reactions between PuO_2 and Ag^{2+}:

$$PuO_2 + Ag^{2+} \longrightarrow PuO2^{+} + Ag^{+} \quad (1)$$

$$PuO_2^{+} + Ag^{2+} \longrightarrow PuO_2^{2+} + Ag^{+} \quad (2)$$

with the overall result

$$PuO_2 + 2Ag^{2+} \longrightarrow PuO_2^{2+} + 2Ag^{+} \quad (3)$$

It has been argued [1–4], that the monoelectronic redox reaction is much more probable than a redox reaction involving the simultaneous exchange of two electrons. Consequently, the dissolution proceeds through the reaction (1) producing an unstable plutonium(V) ion. The latter immediately reacts with a next available Ag(II) ion to form a stable plutonyl(VI) ion according to reaction (2). As it takes place in the solution, the second reaction is fast.

The key question is where reaction (1) takes place. If it occurs on the surface of PuO_2, then the rate-limiting step must be associated either with the reaction itself or with the diffusion of reactants or products between the bulk and the surface. if reaction (1) takes place in the liquid phase, then the dissolution of PuO_2 in HNO_3 could be the rate-limiting step.

Consider, as a reference, PuO_2 with a specific surface of 2.2 $m^2\ g^{-1}$, for which electrochemical dissolution rates up to 1.8×10^{-3} mg $cm^{-2}\ min^{-1}$ are on record [1]. Assume first that reaction (1) takes place in solution. This means that PuO_2 first has to dissolve in HNO_3. In pure nitric acid solutions, PuO_2 is, for all practical purposes, insoluble. Its thermodynamically calculated solubility in 4 M HNO_3, for instance, is only 0.06 g l^{-1} [5] and is consistent with the values of 0.03 g l^{-1} to 0.07 g l^{-1} determined experimentally in the same work. Nevertheless, so long as this (admittedly low) solubility is finite, there is a corresponding driving force for PuO_2 dissolution. Reaction (1) would then be needed only to sustain this small driving force through scavenging PuO_2 from solution by forming plutonyl. However, the published rates of PuO_2 dissolution in pure 4 M HNO_3 ranging from a low of 2.6×10^{-7} mg $cm^{-2}\ min^{-1}$ [5] to a high of 1.5×10^{-5} mg $cm^{-2}\ min^{-1}$ [6] are two to four orders of magnitude lower than the above reference rate. It is clear that this high rate would not be possible if Ag^{+2} ions had to wait first for PuO_2 to dissolve before reacting with it. Reaction (1) therefore must be taking place at the surface.

Suppose now that the diffusion of plutonyl between the bulk and the surface is the rate-limiting step. For PuO_2 with a specific surface of about 2.2 $m^2\ g^{-1}$ the average particle size d_p should be around 0.23 $\mu m = 2.3\times10^{-3}$ cm, assuming uniform spheres. A conservative estimate of mass transfer coefficient k_D, based on the Sherwood number $Sh = k_D d_p/D = 2$ for stagnant media and the above particle size, would give

$$k_D = \frac{2D}{d_p} \approx 0.87\ cm^{-1}\ s^{-1} \approx 50\ cm\ min^{-1}$$

where the typical diffusivity in aqueous solutions $D \approx 10^{-5}\ s^{-1}$. With a mass transfer coefficient of such a magnitude, the observed electrochemical dissolution rate of 1.8×10^{-3} mg $cm^{-2}\ min^{-1}$ is attained easily at a plutonyl concentration difference of only 3.6×10^{-5} g l^{-1} or 1.3×10^{-7} M. This shows that plutonyl diffusion is, in fact, so intense as virtually to eliminate its concentration differential between the surface and the bulk. The same reasoning rules out other possible external diffusion limitations for at least as long as the particles are small, leaving us just one possibility — that reaction (1) occurs on the surface of PuO_2 particles and is rate limiting.

A similar mechanism involving two one-electron-transfer steps was also confirmed [7] in the case of homogeneous oxidation of formic acid by Ag(II). Importantly, the formation of the formyl free radical in the first rate-limiting step was shown to be first order in Ag(II). This makes a strong case for the first-order (or pseudo-first-order) kinetics governing the formation of plutonyl(V). The rate of plutonium oxide dissolution will therefore be described

by the following equation:

$$\frac{dm}{dt} = -kS[\text{Ag(II)}] \tag{4}$$

Here m is the mass of the dissolving plutonium oxide, S is its surface area, [Ag(II)] is the concentration of Ag(II) and k is the as yet unknown first-order rate constant.

In the special case of material consisting of uniform spherical particles their surface would change during dissolution in the following manner:

$$S = S_0 \left(\frac{m}{m_0}\right)^{2/3} \tag{5}$$

with the initial surface S_0 given by

$$S_0 = \frac{6m_0}{\rho d_{p0}} \tag{6}$$

Here m_0 and d_{p0} are the initial mass and particle size and $\rho = 11.5$ g cm^{-3} is the PuO_2 density.

If, in addition, Ag(II) concentration is held constant during dissolution, eqn. (4) can be integrated:

$$\int_{m_0}^{m} m^{-2/3}\, dm = -k[\text{Ag(II)}] \frac{S_0}{m_0^{2/3}} \int_0^t dt \tag{7}$$

yielding the relationship between the dissolution time t and the fraction of dissolved material $X = 1 - m/m_0$:

$$t = \frac{3[1-(1-X)^{1/3}]m_0}{kS_0[\text{Ag(II)}]} = \frac{[1-(1-X)^{1/3}]\rho d_{p0}}{2k[\text{Ag(II)}]} \tag{8}$$

The time τ required to complete dissolution ($X = 1$) is thus

$$\tau = \frac{3m_0}{kS_0[\text{Ag(II)}]} = \frac{\rho d_{p0}}{2k[\text{Ag(II)}]} \tag{9}$$

For uniform spherical particles dissolving at a constant Ag(II) concentration, eqns. (8) and (9) provide a basis for determination of the rate constant k. In practical applications, however, these conditions are not usually met. The linear shape of the electrochemical dissolution curves mentioned earlier indicates that, even though the particle size and Ag(II) concentration were changing in the process, the dissolution rates of PuO_2 remained nearly constant. Given the structure of the right-hand side of eqn. (4), this is only possible if the product S[Ag(II)] itself was constant.

The coupling of the Ag(II) concentration and the surface area S, occurring along linear parts of the dissolution curves, is caused by a combination of two factors: the high reactivity of the material and the limited rate of replenishment of Ag^{2+} ions. This reduces the equilibrium concentration of

Ag(II) well below the upper limit corresponding to the total Ag concentration (even after the effect of Ag(II) reaction with water is taken into account) and keeps the Ag(I) concentration near its initial level. The latter explains the constant electrolytic cell output and the former makes it a controlling factor. As a result, for example the higher anodic current can increase the bulk Ag(II) concentration, leading to a higher dissolution rate, while higher material reactivity (either through k by, for example, increasing the temperature, or through S by increasing the amount of PuO_2 or using finer particles) would only further deplete the solution of Ag(II) ions, leaving the dissolution rate unchanged. In other words, whenever Ag(II) generation controls the electrochemical dissolution rate, Ag(II) concentration acts as a buffer adjusting to any change in k or S in such a way as to keep the right-hand side of eqn. (4) approximately constant.

This has important implications. The linear parts of dissolution curves are not suitable for the determination of the rate constant because widely different k values would fit the same data. The ideal situation for evaluation of the rate constant experiment would satisfy the conditions that led to eqns. (8) and (9) but, because in most real experiments [Ag(II)] varies to some degree, a numerical simulation is required. To illustrate this, the conditions of the experiment reported by Bourges *et al.* [1] were modified in the model (described in the following section) to reduce the rate of Ag(II) generation approximately tenfold. The results of this exercise, which are shown in Fig. 1, confirm that, as long as the product S[Ag(II)] remains constant, the dissolution kinetics do follow straight lines which are almost indistinguishable despite the different values of the rate constant k.

In view of what has been said, the experimental plots of dissolution *vs.* time exhibiting maximum curvature were sought for numerical simulation. One such plot with distinctive curvature above about 75% dissolution stands out among the many reviewed here. It was obtained by Bourges *et al.* [1]

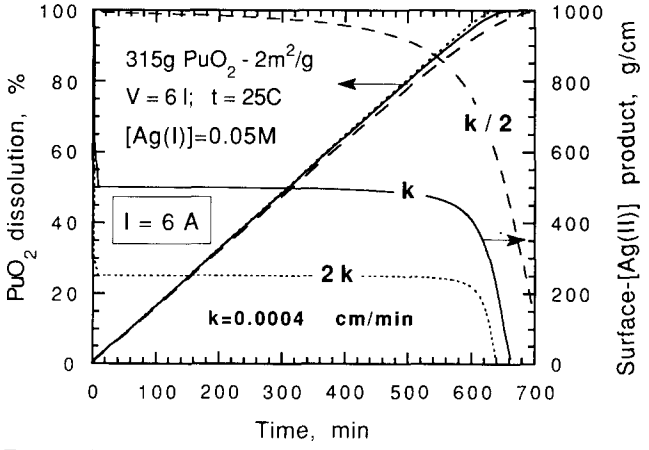

Fig. 1. Ambiguity in determination of the rate constant k due to Ag(II) concentration and PuO_2 surface area coupling when Ag(II) generation controls the dissolution rate.

from the results of a large-scale experiment with a powerful electrolytic cell and is reasonably well documented by these workers. This plot, shown in Fig. 2, has been selected and is used throughout the present study.

3. Numerical simulation of the experiment of Bourges *et al.*

A plot of PuO_2 dissolution *vs.* time, which is depicted in Fig. 2, has been obtained by dissolving 315.2 g of PuO_2 in 6 l; the apparatus is shown in Fig. 3. The apparatus consisted of the dissolution compartment and the electrolytic cell with forced solution circulation between the two within the

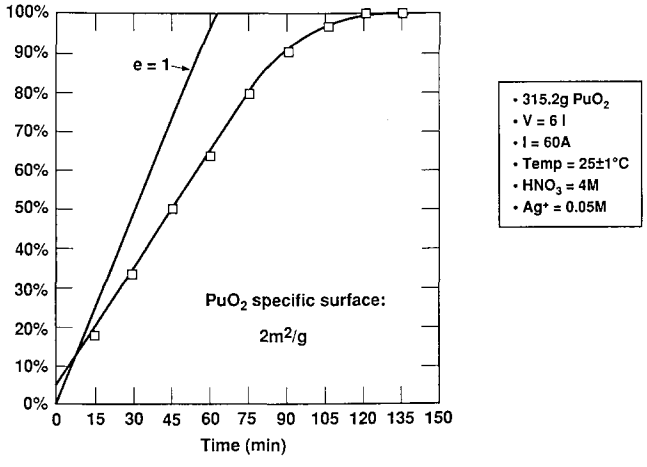

Fig. 2. A Bourges *et al.* [1] plot of PuO_2 dissolution *vs.* time used for the rate constant k fitting.

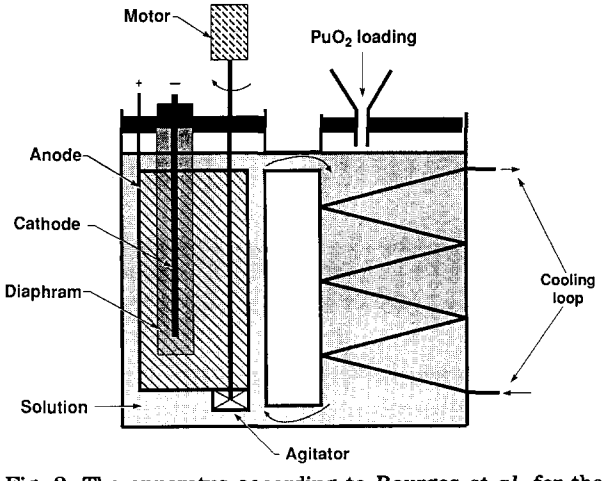

Fig. 3. The apparatus according to Bourges *et al.* for the PuO_2 dissolution experiment used for mathematical simulation.

same enclosure. It was therefore reasonable to treat the entire apparatus in the model as a single volume. The reported conditions of the experiment are summarized in Table 1.

As the earlier discussion made clear, the need to follow the change in Ag(II) concentration during dissolution is the prime reason for modeling. Such information is derived from a solution of the material balance accounting for all essential sources and sinks of Ag(II) ions within a system. For the apparatus used by Bourges *et al.* [1] the material balance with respect to silver(II) takes the following form:

$$V\frac{d[Ag(II)]}{dt} = R_{gen} - R_{H_2O} - R_{PuO_2} \qquad \text{mol s}^{-1} \tag{10}$$

Here V is the apparatus volume, R_{gen} is the rate of Ag(II) generation by the electrolytic cell, R_{H_2O} is the rate of Ag(II) consumption through the reaction with water and R_{PuO_2} is the rate of Ag(II) consumption by the plutonium oxide.

Oxidation of Ag^+ to Ag^{2+} at the anode is a fast process and the rate of diffusion of Ag^+ ions from the bulk to the anode surface determines the apparent rate of Ag(II) generation. With adequate agitation, the diffusion control is largely localized within a narrow zone adjacent to the anode – the diffusion boundary layer. The conductance of this layer is usually quantified by means of a mass transfer coefficient k_D, in units of centimeters per second, leading to the expression below, describing the diffusion flux of silver(I) to the anode:

$$j_D = 10^{-3}k_D\{[Ag(I)] - [Ag(I)]_s\} \qquad \text{mol s}^{-1}\ \text{cm}^{-2} \tag{11}$$

The factor 10^{-3} in (11) converts liters to cubic centimeters. Here $[Ag(I)]_s$ is the Ag(I) concentration at the anode surface at a given current. In the absence of a current $[Ag(I)]_s = [Ag(I)]$, and the diffusion flux terminates. At the other extreme, with too high a current, $[Ag(I)]_s \to 0$, and the flux reaches its upper limit determined only by the hydrodynamic conditions in the cell. However, a fraction of the current in this case is likely to be wasted on reactions other than Ag(I) oxidation, causing the current efficiency e to fall below 1. For a given [Ag(I)] there is therefore a current capable of delivering that maximum flux with the efficiency still close to 1. This limiting current, which is optimum from the Ag(II) generation standpoint, is given by

$$I_{lim} = 10^{-3}FAk_D[Ag(I)] \qquad \text{A} \tag{12}$$

TABLE 1

Reported conditions for the experiment of Bourges *et al.* [1]

m_0 (g)	V (l)	A (cm^2)	I (A)	T (°C)	$[Ag(I)]_0$ (M)	$[HNO_3]$ (M)
315.2	6	1000	60	25 ± 1	0.05	4

where $F = 96\ 487$ C mol^{-1} is the Faraday constant and A is the anode surface area. At any current $I \leqslant I_{lim}$ the cell efficiency $e = 1$. Once the current I exceeds I_{lim}, its efficiency drops:

$$e = \frac{I_{lim}}{I} < 1 \tag{13}$$

With the wire mesh anode surface $A = 1000$ cm^2 in the pilot-scale apparatus, Bourges *et al.* [1] reported $I_{lim} = 80$ A at [Ag(I)] = 0.05 M. According to (12), the mass transfer coefficient $k_D \approx 0.016$ cm s^{-1} for this anode, which is an order of magnitude larger than a typical value for a solid anode of a comparable size.

With the above value of k_D, the Ag(II) generation term R_{gen} in the material balance (10) can be expressed in the form used in the model:

$$R_{gen} = \frac{eI}{F} \quad \text{mol s}^{-1} \tag{14}$$

The second term in (10) accounts for Ag(II) losses due to its reaction with water. The kinetics of Ag(II) reduction by water have been established by Po *et al.* [8]:

$$R_{H_2O} = Vk_{H_2O}[\text{Ag(II)}]^2 \quad \text{mol s}^{-1} \tag{15}$$

where

$$k_{H_2O} = \frac{4\alpha}{1 + \beta[H^+]^2[\text{Ag(I)}]} \quad \text{l s}^{-1}\ \text{mol}^{-1} \tag{16}$$

is a second-order rate constant for this reaction which takes into account the effects of Ag(I) concentration and the solution acidity. The temperature effect, very pronounced at elevated temperatures, is entered into (16) by means of two coefficients α and β:

$$\alpha = \exp\left(-10.919 + \frac{7921.3}{1.987T}\right) \quad \text{l s}^{-1}\ \text{mol}^{-1}$$

$$\beta = \exp\left(-48.254 + \frac{32764}{1.987T}\right) \quad \text{M}^{-3}$$

The rate of Ag(II) consumption by the plutonium oxide is stoichiometrically related to the rate of its dissolution, given in (4). According to the overall stoichiometry of PuO_2 dissolution shown in (3), two moles of Ag(II) are consumed by each mole of PuO_2 dissolved. Therefore the last term in (10) is

$$R_{PuO_2} = 2\frac{dm}{dt} \quad \text{mol s}^{-1} \tag{17}$$

Summing (14), (15) and (17) yields the net change in Ag(II) concentration in the system as dissolution proceeds:

$$\frac{d[Ag(II)]}{dt} = \frac{eI}{VF} - k_{H_2O}[Ag(II)]^2 - \frac{2}{V}\frac{dm}{dt} \quad M\ s^{-1} \tag{18}$$

Virtually all parameters in (12) and (13) are fixed during normal cell operation except [Ag(I)]. Within a fixed volume V assumed in the model, Ag(I) concentration must balance the difference between its initial concentration $[Ag(I)]_0$ and the concentration of Ag(II):

$$[Ag(I)] = [Ag(I)]_0 - [Ag(II)] \tag{19}$$

Consequently, depending on the relative rates of Ag(II) generation and consumption, [Ag(I)] can vary from the maximum of $[Ag(I)]_0$ to much lower values. A cell operated at a limiting current would respond to such [Ag(I)] variation in a manner specified by (12). Alternatively, when the current is fixed, as in the experiment modeled here, its efficiency follows the limiting current according to (13). Consistent with the approach of Bourges *et al.* [1], the current efficiency defined here is the fraction of a current which is productive and leads to generation of Ag(II). It should not be confused with a system efficiency which, in addition, accounts for further losses of Ag(II) within the system after it has been generated. The system efficiency is therefore always lower than the current efficiency.

At each time step, eqn. (18), with updated current efficiency (by means of (19), (12) and (13)) and rate of PuO_2 dissolution, is solved for [Ag(II)]. This new Ag(II) concentration, together with a new value of S are, in turn, used in eqn. (4) to obtain a new rate of PuO_2 dissolution. This brings up the important issue of the material surface area S and its change in the process.

The plutonuim oxide was prepared for the experiment by Bourges *et al.* [1] by calcining plutonium oxalate at 1000 °C but, besides the calcination temperature, neither the specific surface nor the size distribution of their product was reported. The lacking information was filled in with the results of Brunauer–Emmett–Teller surface measurements performed elsewhere [2, 4, 5] on similarly prepared PuO_2 samples. A strong effect of calcination temperature on the specific surface of PuO_2 is evident in Fig. 4 representing an exponential least-squares fit (with a regression coefficient of -0.961) of the data collected from the above references. This treatment provided a rough estimate for the specific surface of material used in ref. 1 and was assumed to be 2.0 $m^2\ g^{-1}$ for the numerical simulation of their experiment.

At the onset of dissolution, the initial surface S_0 of the plutonium oxide is evaluated as a product of its initial mass m_0 and the specific surface. If a material to be dissolved were uniform spheres, then from eqn. (6) its initial size would have been $d_0 \approx 0.26$ μm and its surface would change during the dissolution according to eqn. (5). However, the existing data are insufficient for such an assumption. Consequently, the model was made capable of processing n different size fractions, each consisting of spherical particles of equal size $d_0(i)$ $(1 < i < n)$. Regardless of the size distribution, however, their total initial specific surface always summed to 2.0 $m^2\ g^{-1}$.

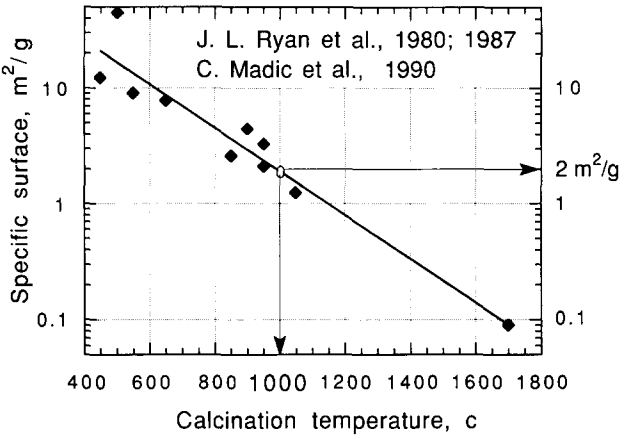

Fig. 4. Reported specific surface of PuO_2 prepared from oxalate as a function of the oxalate calcination temperature.

The surface and the dissolution rate in the model are therefore computed for each individual size fraction:

$$S(i) = S_0(i) \left(\frac{m(i)}{m_0(i)} \right)^{2/3} \qquad \text{cm}^2 \tag{20}$$

where

$$S_0(i) = \frac{6m_0(i)}{\rho d_0(i)} \qquad \text{cm}^2 \tag{21}$$

and

$$\frac{\mathrm{d}m(i)}{\mathrm{d}t} = -10^{-3} k S(i)[\text{Ag(II)}] \qquad \text{mol s}^{-1} \tag{22}$$

In order to follow the diminishing surfaces $S(i)$ of n size fractions based on their remaining masses $m(i)$, the rates $\mathrm{d}m(i)/\mathrm{d}t$ of their disappearance, as the dissolution progresses, have to be followed first. Upon computation of the right-hand sides of eqns. (22), the new masses $m_{j+1}(i)$ are obtained by integrating (22) over the time interval Δt:

$$\int_{m_j(i)}^{m_{j+1}(i)} \mathrm{d}m(i) = -r_j(i) \int_{t_j}^{t_{j+1}} \mathrm{d}t \tag{23}$$

with the value of $r_j(i)$ being the result of previous computation of the right-hand side of (22):

$$m_{j+1}(i) = m_j(i) - r_j(i) \qquad \Delta t \tag{24}$$

These new masses of the size fractions are used in (20) to update their surfaces. Once all surfaces $S(i)$ are known, eqns. (22) are summed prior to their use in (18):

$$\frac{dm}{dt} = \sum_{i=1}^{n} \frac{dm(i)}{dt} \tag{25}$$

A third-order Runge–Kutta procedure (see the work by Carnahan *et al.* [9]) was implemented for the numerical integration of eqn. (18):

$$[\text{Ag(II)}]_{j+1} = [\text{Ag(II)}]_j + \frac{\Delta t}{6}(k_1 + 4k_2 + k_3) \tag{26}$$

where

$$k_1 = f([\text{Ag(II)}]_j) \tag{27}$$

$$k_2 = f\left([\text{Ag(II)}]_j + \frac{\Delta t\, k_1}{2}\right) \tag{28}$$

and

$$k_3 = f([\text{Ag(II)}]_j + 2\,\Delta t\, k_2 - \Delta t\, k_1) \tag{29}$$

The function f is formed by the right-hand side of eqn. (18).

4. Results and discussion

The model described in the previous section with the design and operational parameters listed therein was used for simulation of the PuO_2 dissolution experiment of Bourges *et al.* [1]. Besides the size distribution, whose variation, however, was restricted by a fixed specific surface constraint, the only free parameter in the model was the rate constant k whose values were independently picked in a series of simulation runs aimed at matching the experimental dissolution curve shown in Fig. 2. Our simulation followed the actual procedure in which the experimental cell was allowed to run for approximately 5 min prior to the introduction of PuO_2. The initial build-up of Ag(II) in the system caused the dissolution to start at a rate noticeably faster than was more typical for the run. Besides matching the original and the simulated dissolution curves, the calculated average current efficiency was also checked against its reported counterpart, which gave us one more criterion of successful simulation.

Following this approach, the best fit to the data was found for $k = 0.0004$ cm min^{-1}. The results of that simulation run (full curve) are shown in Fig. 5. In addition to a good fit to data achieved with the above k value, the average current efficiency was also closely matched. Surprisingly, this match, obtained with material of uniform size $d_0 = 0.26$ μm, turned out to be superior to any obtainable with distributed sizes. The uniqueness of the numerical value found for k is evident after k is halved (broken line) or doubled (dotted line), causing the dissolution rate to respond accordingly. This "high resolution" in evaluation of the rate constant was made possible by the relatively high rate of silver(II) generation with respect to its consumption, confirming

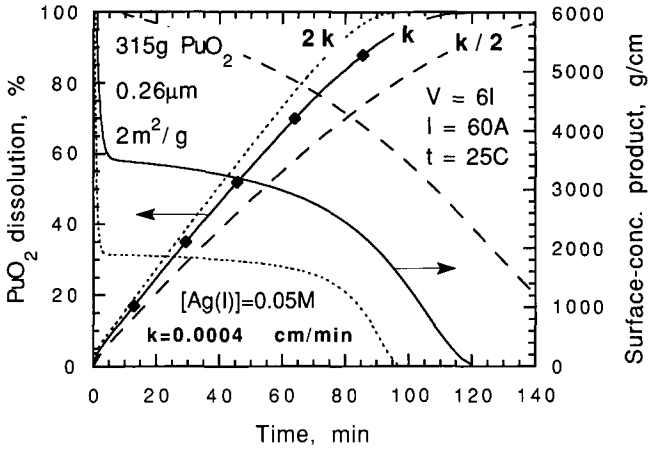

Fig. 5. Fitting the rate constant k to the data (♦) in Fig. 2 obtained at fixed anodic current of 60 A, assuming PuO_2 particles of uniform size.

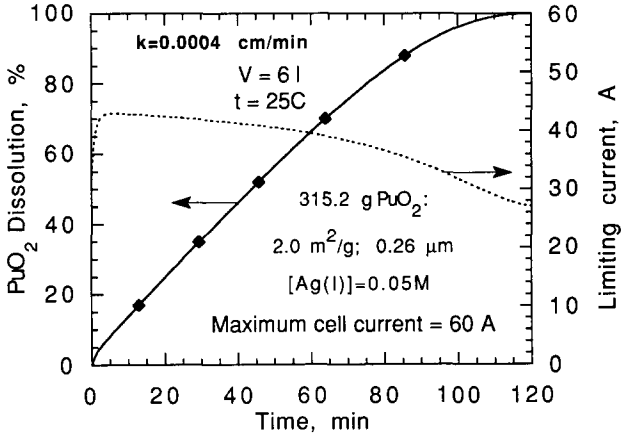

Fig. 6. Fitting the rate constant k to the data (♦) in Fig. 2 using the limiting current.

our choice of the experiment. It should be compared with the hypothetical "poor experiment" in Fig. 1 in which the Ag(II) generation rate was an order of magnitude lower. As in Fig. 1, the relationship between the linearity of the dissolution curves and the coupling of the PuO_2 surface and Ag(II) concentration is clearly evident in Fig. 5.

The experiment modeled in Fig. 5 was conducted at constant 60 A current, while the reported current efficiency averaged around 64%. The same results, obviously, could have been achieved with 100% current efficiency if the cell operated at the limiting current. In this case, shown in Fig. 6, the experimental data of ref. 1 are reproduced using on average only two thirds of the actual current.

The effect of size distribution is demonstrated in Fig. 7. It shows how different simulation runs with the same PuO_2 specific surface but progressively

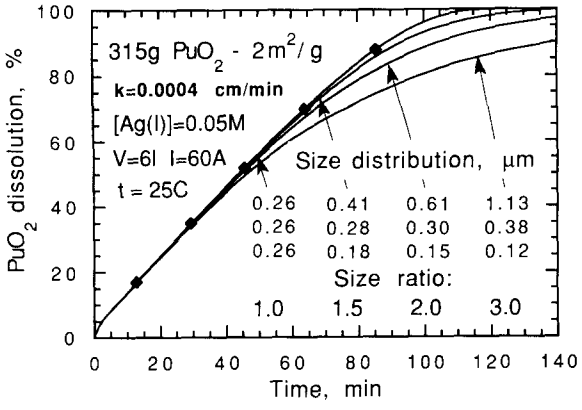

Fig. 7. Fitting the rate constant k to the data (◆) in Fig. 2 assuming polydispersed PuO_2 particles.

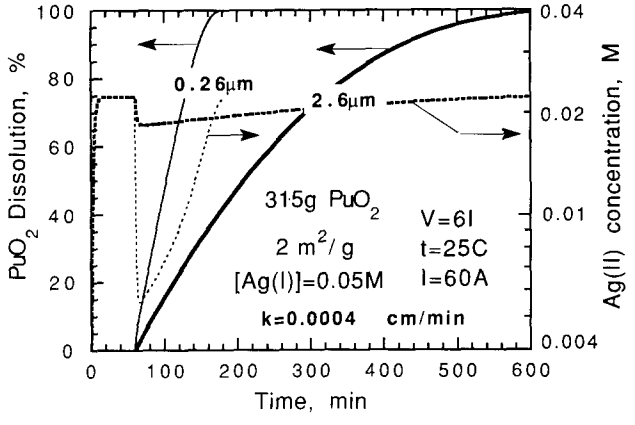

Fig. 8. Effect of PuO_2 reactivity (particle size) on its dissolution time and Ag(II) concentration.

wider size distributions deviate from the data. In each run the PuO_2 load was composed of three equal weight fractions where the particle sizes followed a geometric progression with the common ratios of 1 (uniform size), 1.5, 2 and 3.

With the dissolution model proved and the value of the rate constant established, the model can be explored to obtain a better insight into complex interactions among principal process parameters. In Fig. 8 and Fig. 9, PuO_2 was loaded after the cell was run for 1 h. The steady state Ag(II) concentration in Fig. 8 is achieved after operation for only 10 min but remains well below the total silver concentration because of the Ag(II) reaction with water. It drops sharply further once highly reactive 0.26 μm PuO_2 has been loaded (dotted curve). A similar but much smaller drop occurs in the case of the ten times coarser 2.6 μm PuO_2 (broken curve). The dissolution curves are represented in Fig. 8 by thin and bold full curves. The complete dissolution

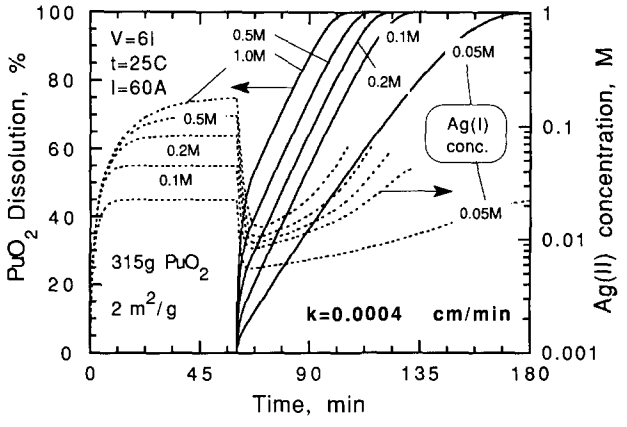

Fig. 9. Effect of total silver concentration (initial Ag(I) concentration) on PuO_2 dissolution time and Ag(II) concentration.

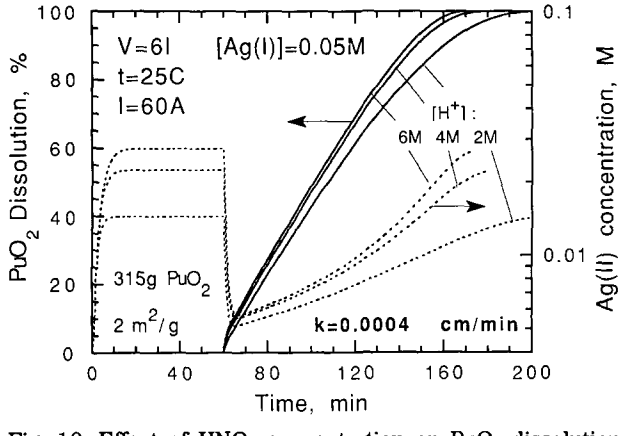

Fig. 10. Effect of HNO_3 concentration on PuO_2 dissolution kinetics.

times for two sizes differ by a factor of 5. According to eqn. (9), this factor would have been 10 if the Ag(II) concentration were the same in both cases.

The effect of the Ag(I) concentration on dissolution of 0.26 μm PuO_2 at fixed anodic current is depicted in Fig. 9. The initial Ag(I) concentration was varied here in five increments between 0.05 and 1.0 M. The initial silver(II) concentration build-up during the first hour is shown on the left (broken curves). Again, the addition of PuO_2 causes a sharp decrease in Ag(II) concentration and the linearity of the dissolution curves (full curves) is most pronounced when Ag(II) concentration is a minimum. With an anodic current of 60 A, the maximum effect from the increase in silver concentration is realized between 0.05 and 0.1 M. Once the current efficiency reaches 100% at $[Ag(I)] \approx 0.1$ M and beyond, a further modest gain in dissolution rate occurs only as a result of lower water reaction rate constant given by

(16). Even at the risk of higher losses to water reaction, much higher overall dissolution rates could have been realized by boosting the anodic current in proportion to the Ag(I) concentration beyond [Ag(I)] = 0.1 M.

The effect of solution acidity on the PuO_2 dissolution kinetics is pronounced only at the lower end of H^+ concentration and, as is evident in Fig. 10, becomes negligible above $[H^+] = 4$ M. The latter value, commonly regarded as optimum, is therefore justified.

5. Conclusions

This study demonstrates that the electrochemical dissolution of plutonium oxide in the presence of Ag(II) ions is by no means instantaneous. It brings to light the importance of the role played by plutonium oxide dissolution kinetics and shows how the kinetic information can be extracted from the experimental data. The model developed in the process reveals the complexity of interaction between the key process parameters and lays out a theoretical groundwork for understanding the mechanism(s) of electrochemical dissolution of plutonium oxide as well as the oxides of some other actinides. In particular, it demonstrates the strong effects of the PuO_2 size, the Ag(I) concentration and the anodic current on the dissolution time and the current efficiency and stresses the importance of operation at the limiting current. The results of this investigation provide a means for rational design and operation of full-scale plutonium processing units at Lawrence Livermore National Laboratory as well as other US Department of Energy facilities.

Acknowledgment

This work was performed under the auspices of the US Department of Energy by the Lawrence Livermore National Laboratory under Contract W-7405-ENG-48.

References

1 J. Bourges, C. Madic, G. Koehly and M. Lecomte, *J. Less-Common Met.*, *122* (1986) 303–311.

2 E. J. Wheelwright, L. A. Bray and J. L. Ryan, Development of the CEPOD process for dissolving plutonium oxide and leaching plutonium from scrap or wastes, *1987 Prog. Rep. PNL-6483*, Pacific Northwest Laboratory, March 1988.

3 L. A. Bray and J. L. Ryan, Actinide recovery from waste and low grade sources, in J. D. Navratil and W. W. Schulz (eds.), *Radioactive Waste Management*, Vol. 6, Harwood, London, 1982, p. 129.

4 C. Madic, P. Berger and X. Machuron-Mandar, Plutonium dioxide–mechanisms of the rapid dissolutions in acidic media under oxidizing or reducing conditions, *50th Anniversary of the Discovery of Transuranium Elements, Washington, DC, August 27–30, 1990.*

5 J. L. Ryan and L. A. Bray, *Am. Chem. Soc. Symp. Ser.*, *117* (1980) 499–514.

6 D. E. Horner, D. J. Crouse and J. C. Mailen, *USERDA Rep. ORNL/TM-4716*, 1977 (Oak Ridge National Laboratory) (US Energy Research and Development Administration).
7 L. Miller and J. I. Morrow, *Inorg. Chem.*, *15* (1976) 1797–1799.
8 H. N. Po, J. H. Swinehard and T. L. Allen, *Inorg. Chem.*, *7* (1968) 244–249.
9 B. Carnahan, H. A. Luther and J. O. Wilkes, *Applied Numerical Methods*, Wiley, New York, 1969, p. 363.